CHAPTER 1

INTRODUCTION

Diffusion and inter-diffusion between different solids has long been a subject of scientific studies going back to the last century. *Roberts-Austen* carried out one of the first quantitative investigations in 1896, when he reported his work on the fast diffusion of gold into solid lead at different temperatures [1]. He estimated the rate of gold diffusion by measuring the weight change after sectioning the lead. Diffusion history is reviewed in refs. [2,3]. Over the last 100 years many researchers studied inter-diffusion of solids and many different models of diffusion mechanisms were developed.

In recent years with the rapid development of semiconductors, diffusion became of great technological importance for manufacturing *p-n* junctions in elementary semiconductors. Different diffusion models in solids and in particular in semiconductors are discussed in chapter 2.

Aluminium is still widely used for contacts on semiconductors. As a group *III* element it can also be used as an acceptor for group *IV* elemental semiconductors.
In the present work the diffusion of aluminium in different semiconductors was investigated. For analysing the in-diffusion, aluminium films were deposited onto clean silicon, germanium, gallium arsenide, indium phosphide and indium antimonide surfaces. To activate a possible in-diffusion, the semiconductor samples were annealed in vacuum at different temperatures. Depth profiles before and after every annealing step were compared to extract diffusion coefficients.

Further research was done on the aluminium diffusion within these semiconductors. Clean samples of the above mentioned semiconductors were implanted with aluminium at room temperature and at T_i = 250 °C at different dose rates. These samples were annealed for one hour in vacuum at different temperatures. The depth profiles of aluminium after implantation and after every annealing step were compared and diffusion coefficients were extracted.

The aluminium depth profiles were obtained by nuclear reaction analysis (NRA) by making use of the narrow $^{27}Al(p,\gamma)^{28}Si$ reaction at a proton energy of 992 keV. This non-destructive method has various advantages over other methods like Rutherford backscattering (RBS), as it is isotope sensitive and light elements in a heavy bulk can be analysed. In some of the analysed systems channeling measurements in backscattering geometry were performed to obtain additional information on radiation induced damage in the surface region of the specimen.

Chapter 3 summarises the concept of stopping powers of ions in solids. The p-γ resonance reaction applied in this research is described in chapter 4. Chapter 5 is on the experimental set-up as well as the sample preparation for the different diffusion experiments. The automatic energy scanning system, which provided a convenient tool for depth profiling with NRA is explained. The channeling of α - particles to determine the radiation induced damage before and after the different annealing steps is briefly discussed.

In chapter 6 previously published results in this field of research are reviewed. The discussion of the diffusion results of aluminium in the investigated semiconductors is presented in Chapter 7. Chapter 8 summarises the results of this work and gives a brief outlook.

CHAPTER 2

DIFFUSION

Heat conductivity, viscosity and diffusion are transport phenomena. Hence, the existing diffusion theories are derived from theories of heat flow through solid media that date back to Fourier and Lord Kelvin. In a diffusion process atoms or molecules are transported from a region of higher concentration to a region of lower concentration in a system, which can be of gaseous, liquid or solid nature. Diffusion alters physical and chemical properties of a system. It increases with temperature and can be enhanced by irradiation.

A proper study of diffusion mechanisms as well as diffusion coefficients for different systems is therefore necessary to predict modifications of solids in a hot or radioactive environment.

More recent diffusion studies are on semiconductor – impurity systems to predict their long time thermal stability [4].

2.1. DIFFUSION COEFFICIENT

Fick's first law of diffusion [5,6] macroscopically connects the diffusion coefficient D and the gradient of the concentration C to the flow rate J. In the differential form it can be written as:

$$J = -D\, grad\, C \tag{1}$$

In equation 1 the transfer rate of atoms per unit area is calculated. The definition constitutes the theoretical basis of most experimental methods for determining diffusion coefficients in generally used methods such as the chemical and tracer techniques and the *p-n-* junction method which is a specific method for semiconductors (chapter 2.3.).

Ficks's second law, also called the general diffusion equation, can be derived from equation (1) by assuming diffusion in the positive x - direction of a cylinder of unit cross section. From the continuity equation:

$$\frac{\partial C}{\partial t} + div\, J = 0 \tag{2}$$

Fick's second law can be derived after inserting equation (1):

$$\frac{\partial C}{\partial t} = D\ div\ grad\ C = D\, \nabla^2 C \tag{3}$$

The solutions of these differential equations depend strongly on the boundary conditions of an experiment. Equation (3) is often expressed in spherical polar co-ordinates and in cylindrical co-ordinates [7] depending on the geometry of the experimental set-up.
For a semi-infinite medium equation (3) can be analytically solved [7]:

$$C(x,t) = \frac{1}{2\sqrt{\pi D t}} \int_0^\infty C(\xi,0) \left[\exp\left(-\frac{(\xi - x)^2}{4Dt} \right) \pm \exp\left(-\frac{(\xi + x)^2}{4Dt} \right) \right] d\xi \tag{4}$$

where $C(\xi,0)$ is the initial distribution. The positive sign is for a reflecting surface, the negative sign for a permeating surface.

For high temperatures the diffusion coefficient is found to obey an Arrhenius equation:

$$D(T) = D_0 \exp\left(-\frac{E_A}{kT}\right) \tag{5}$$

with the Boltzmann constant k and the Temperature T in units of Kelvin. Here the diffusion is characterised by just two quantities, the pre-exponential factor or diffusion constant D_0 and the activation energy for diffusion E_A.

2.2. DIFFUSION MECHANISMS IN SOLIDS

An ideal crystal consists of a perfectly ordered array of atoms, ions, or molecules in three dimensions. There cannot be atomic diffusion in a perfect lattice, which conserves its ideal order under all circumstances. But most crystals are far from being ideal. An actual evidence of the fact that crystals are not ideally ordered under all conditions lies in the existence of diffusion.

Existing defects in a crystal can be vacancies (Schottky-defects) or displaced atoms from their regular lattice sites to interstitial sites. Such an interstitial atom together with its vacated lattice site is called a Frenkel-pair. Extended defects in a crystal are agglomerates of vacancies (point defect clusters) or interstitials, dislocations and grain boundaries.

Investigations on point defects in a crystal can be performed after their artificial creation, which is achieved by quenching from high temperatures, through plastic deformation or after irradiation with particles or γ-rays [8].

Some interstitial sites and most of the above mentioned defects are locations of minimum energy for displaced and for impurity atoms. For an atom to move from one of these sites to another site of minimum energy a certain amount of energy, the so-called activation energy is required. A vacated lattice site (vacancy) can also start to move or diffuse when energy above a threshold energy is applied. However, the migration energy for vacancies in a solid is much larger than that for interstitials ($E_{AV} >> E_{AI}$).

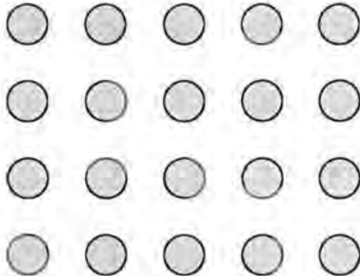

Fig.1: Undisturbed lattice

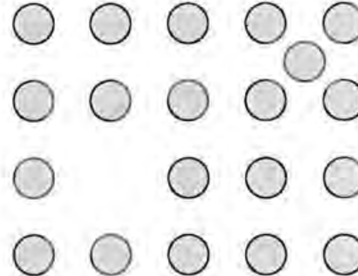

Fig.2: Frenkel disorder in a two dimensional lattice.

In thermal equilibrium the number of vacancies n in a solid with N atoms is given by:

$$\frac{n}{N-n} = \exp(-E_V / k_B T) \qquad (6)$$

where E_V is the energy to displace one atom from its lattice site to the surface.

Lattice defects and impurities can influence the thermal atomic diffusion in a solid. The diffusing atoms can be trapped at such lattice defects where they can precipitate, segregate or

undergo chemical reactions with the matrix elements. To describe a Fickean diffusion process in the presence of trapping, a source and a sink term have to be added to equation (3):

$$\frac{\partial C_F(x,t)}{\partial t} = D\frac{\partial C_F(x,t)}{\partial x^2} - C_F(x,t)\left(\sum_i \mu_i(x,t)\right) + \sum_i \left(\nu_i C_{T,i}(x,t)\right) \quad (7)$$

C_F and $C_{T,i}$ is the concentration of the free and the trapped atoms respectively. μ_i describes the trapping probability for a certain trapping centre as a function of its radius r_i (typically a few Å) and the concentration of traps F_i:

$$\mu_i = 4\pi r_i D F_i(x,t) \quad (8)$$

ν_i is the dissociation frequency of the complex, which follows an Arrhenius type behaviour:

$$\nu_i = \nu_{i,o}\, e^{-E_i/kT} \quad (9)$$

where $\nu_{i,o}$ is about 10^{13} s^{-1} and E_i is the dissociation energy of the complex, which is typically between 0.8 and 2.5 eV.

The solid solubility of the diffusant in the solid also influences the diffusion behaviour. The diffusion constant depends inversely upon the solid solubility and is therefore small for self-diffusion, where the solute and the solvent are identical and the solute can occupy a regular lattice site without distorting the lattice.

It has become customary to classify impurities into 'slow' and 'fast' diffusers. Diffusion coefficients of 'slow' diffusers are in the same range or at most about 10^2 times higher than the self-diffusion coefficients of the investigated solids. 'Fast' diffusers usually diffuse several orders of magnitudes faster than 'slow' diffusers.

2.2.1. DIFFUSION IN SEMICONDUCTORS

With the importance of the semiconductor technology many diffusion data have been reported over the last years (see chapter 6). Diffusion processes play an important role in

various aspects of modern semiconductor technology. One of the most important applications is the generation of *p-n* junctions by diffusing impurity atoms into semiconductors at elevated temperatures, without melting the crystal or the formation of a liquid alloy. The diffusing impurities are either applied to the semiconductor surface in the gaseous state or as a solid or liquid compound. The depth and the sharpness of the junction can be controlled quite accurately by applying the desired amount of impurity atoms to the surface with a successive heat treatment.

The diffusion data of the elemental semiconductors silicon and germanium are in several respects different from those of metals. In a review on diffusion in silicon and germanium by Seeger and Chik [8] the following was reported on self-diffusion:

i. due to the low point defect concentration in the thermal equilibrium, the self-diffusion in semiconductors is much slower than in metals (more than 10^4 times),
ii. the pre-exponential factor D_0^{SD} is at least 10^2 times larger in germanium and 10^4 times larger in silicon than in metals,
iii. from (i) and (ii) it follows that the activation energies for self diffusion are much larger in silicon and germanium than in metals with comparable melting points.

In semiconductors, intrinsic defects such as vacancies and interstitials may be electrically charged and may therefore strongly interact with impurities such as donors and acceptors. In general, the intrinsic defects may exist in different charge states. The change in the Fermi level due to the addition of electrically active impurities affects the populations of these charge states and may thus have a strong influence on the observed diffusion coefficients.
For the elemental semiconductors silicon and germanium it was found that typical representatives of 'slow' diffusers are group *III* and group *V* elements of the periodic table, i.e. those usually employed as acceptors or donors in *p-n*-junctions. Group *I* and group *VIII* elements constitute the most important 'fast' diffusers. Therefore diffusion coefficients of group *III*- impurities are expected to be of the order of the self-diffusion coefficient (see Chapter 6).

In semiconducting compounds the diffusivity of impurity atoms depends on the vapour pressures of the components, since these have an influence on the concentrations of the various intrinsic point defects.

While in-diffusion is widely used to manufacture *p-n* junctions in elemental semiconductors difficulties of this method can occur in *III-V* device structures. The high vapour pressures of the group *V* elements lead to incongruent evaporation from the surface unless an overpressure or encapsulant is provided [9].

Other doping methods like ion-implantation can be applied for *III-V* semiconductors. The desired impurities are placed into the near surface region of the solid by first accelerating them to a high velocity and directing them as a beam onto the semiconductor surface. The ions are then able to penetrate the solid, and are gradually brought to rest. However, to anneal the damage introduced during the implantation requires displaced atoms to diffuse back to appropriate sites. This is sometimes not possible in *III-V* semiconductors for the diffusion lengths are not large enough to accomplish complete regrowth. An application of this method lies in the production of semi-insulating layers in the surface area of the *III-V* semiconductor.

To avoid extended defects, implantations at elevated temperatures are performed into elemental and compound semiconductors, where due to an increased mobility of point defects radiation induced damage can be largely avoided. This method is also known as dynamic annealing.

2.3. METHODS FOR ANALYSING DIFFUSION COEFFICIENTS

Apart from nuclear reaction techniques, which is used in this study (described in chapter 4) a variety of other methods can be applied to analyse the diffusion behaviour of impurities in solids. A widely used method for diffusion analysis is secondary ion mass spectroscopy (SIMS). In this technique the analysed specimen is subjected to sputtering. The material sputtered from the surface is analysed by mass spectrometry. The concentration of the investigated elements versus the sputter time is recorded from which the depth profiles are calculated.

The tracer method consists of introducing radioactive isotopes of the dopant into the studied solid. Thin layers of the investigated sample are mechanically or chemically removed and the concentration of the isotope in the removed layer is determined by measuring its radioactivity. An advantage of this method is the possibility of self-diffusion studies by using a radioactive isotope of the sample material as a diffusant.

The four-point probe method measures the conductivity of a thin layer just below the surface of a semiconductor. It can be applied in the investigation of concentration profiles of *n*-type dopants in *p*-type substrates or vice versa. Four equally spaced probes are applied to the semiconductor surface. A current I is passed between the two outermost probes and the voltage V between the two probes in the middle is measured. From the geometry of the specimen it is possible to calculate the amount of electrical active dopants. The diffusion profile of the dopant can be obtained by using a sectioning technique.

A similar method is obtained by carrying out the differential Hall measurements rather than simple conductivity measurements. Measurements are again taken before and after stripping thin layers from the diffused specimen. The values for mobility and carrier concentration are obtained at each stage and these data can be converted to a depth profile.

The *p-n*-junction method can be used for diffused acceptors into a homogeneous *n*-type sample. The junction occurs at the depth x_j where the concentration of the acceptors is equal to the concentration of the donors. From the concentration of donors N_D versus the depth x_j in the diffused material the depth profile of the acceptor can be extracted. Diffusion coefficients can be calculated from the difference in shape of the diffused profiles after various annealing temperatures.

2.4. THE FINITE DIFFERENCE METHOD

To evaluate a diffused profile a numerical method based on the finite difference method, described by Crank [10] was applied in this thesis. This method shall be described for a one-dimensional solution of Fick's laws.

For analysing the diffusion in a plane sheet with a constant diffusion coefficient D, the following dimensionless variables are introduced:

$$X=\frac{x}{l}, \qquad T=\frac{Dt}{l^2}, \qquad c=C/C_0 \tag{10}$$

where l is the thickness of the layer. C_0 and C are the initial and the diffused concentration, respectively. Advantages of these substitutions are that numbers occurring in the computation cover roughly the same range for all calculations and that the basic independent parameters are isolated. With these variables Ficks second law can be written as:

$$\frac{\partial c}{\partial T}=\frac{\partial^2 c}{\partial X^2} \tag{11}$$

The variation of an initial distribution $c(X)$ at a time T_0 is obtained by dividing the X-T space into intervals of δX and δT. For every lattice point (X_i,T_j) both sides of equation (11) can be developed by Taylor's expansion theorem. An expression for the left-hand side of equation (11) can be obtained from:

$$c_{i,j+1}=c_{i,j}+\delta T\left(\frac{\partial c}{\partial T}\right)_{i,j}+\frac{1}{2}(\delta T)^2\left(\frac{\partial^2 c}{\partial T^2}\right)_{i,j}+.... \tag{12}$$

when neglecting second and higher order terms equation (12) is written as:

$$\left(\frac{\partial c}{\partial T}\right)_{i,j}=\frac{c_{i,j+1}-c_{i,j}}{\delta T} \tag{13}$$

A similar development leads to the expressions of the right hand side of equation (11):

$$c_{i+1,j}=c_{i,j}+\delta X\left(\frac{\partial c}{\partial X}\right)_{i,j}+\frac{1}{2}(\delta X)^2\left(\frac{\partial^2 c}{\partial X^2}\right)_{i,j}+.... \tag{14}$$

$$c_{i-1,j} = c_{i,j} - \delta X\left(\frac{\partial c}{\partial X}\right)_{i,j} + \frac{1}{2}(\delta X)^2\left(\frac{\partial^2 c}{\partial X^2}\right)_{i,j} - .... \tag{15}$$

and after neglecting third and higher order terms:

$$\left(\frac{\partial^2 c}{\partial X^2}\right)_{i,j} = \frac{c_{i+1,j} - 2c_{i,j} + c_{i-1,j}}{(\delta X)^2} \tag{16}$$

Introducing equations (13) and (16) into equation (11):

$$c_{i,j+1} = c_{i,j} + r\left(c_{i-1,j} - 2c_{i,j} + c_{i+1,j}\right) \tag{17}$$

with $r = \delta T / (\delta X)^2$.

With this the diffused concentration profile at any time can be calculated from the initial profile. This method converges for $r < 0.5$.

The schematic diagram in Fig.3 shows how this method is applied to analyse diffused spectra. After setting the required parameters such as boundary conditions and trapping distribution, a diffused profile is calculated from the initial profile with the finite difference method. This simulated profile is now compared with the experimentally obtained diffused profile. In case of good agreement of the two profiles the product Dt is obtained. In case of disagreement the initial parameters have to be changed and new calculations have to be performed.

For analysis of our depth profiles the computer code DIFFUS by Kashny [11,12] was used.

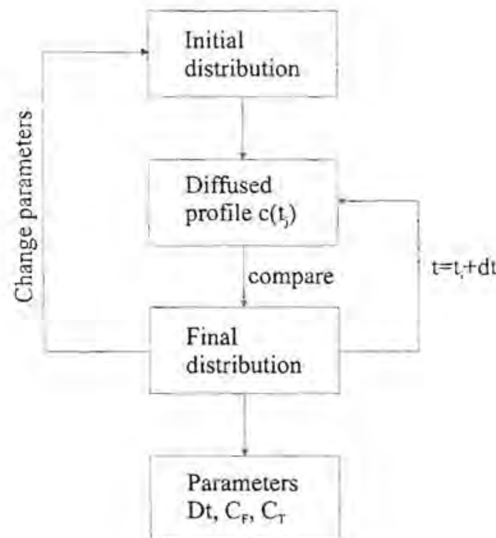

Fig.3: Schematic diagram of the data analysis with DIFFUS. The initially obtained aluminium depth distribution is used as initial distribution from which diffused profiles are calculated with the finite difference method.

CHAPTER 3

STOPPING OF IONS IN SOLIDS

When a charged particle with a certain velocity penetrates a solid, elastic and inelastic collisions with target atoms slow it down. The magnitude of this slowing down depends on the ion, its energy and the target material. For more than the last century stopping powers are of fundamental scientific interest. Various authors developed theories about energy loss mechanisms of charged particles that penetrate a target material. Several approaches are listed in ref.[13].

3.1. ENERGY LOSS

The final range distribution of energetic ions in a solid as well as the defect distribution is determined by the energy loss. The energy loss in a solid dE / dx is often called stopping power or specific energy loss. Here E is the ion energy and x is the distance within the target, usually measured along the instantaneous direction of the ion trajectory.

Two stopping processes that are considered to be ideally independent from each other can be distinguished. These processes are nuclear and electronic stopping. From their sum the total stopping power S is calculated to:

$$S = \frac{dE}{dx} = \left(\frac{dE}{dx}\right)_n + \left(\frac{dE}{dx}\right)_e \qquad (18)$$

The stopping cross section ε is calculated from the stopping power divided by the target density N:

$$\varepsilon = -\frac{1}{N}\frac{dE}{dx} \qquad (19)$$

The relative importance of the interaction process between ion and target medium depends mostly on the ion velocity and the charge state of the ion and target material.

3.1.1. NUCLEAR CROSS SECTION

Nuclear stopping of the projectile is caused from the elastic scattering by the screened atomic potential. At ion velocities v_1, significantly lower than the orbital velocities v_0 of the atomic electrons, the ion becomes neutralised by electron capture. Energy can be transferred from the nucleus of the projectile to that of a target atom by electrostatic interaction between the screened charges of the two nuclei.

The energy transfer T between the projectile and a target atom is calculated from energy and momentum conservation. It is a function of scattering angle θ (in the centre of mass system), projectile energy E, impact parameter b, mass of the projectile (M_1), mass of the target atoms (M_2) and the inter-atomic potential $V(r)$:

$$T(\theta, E) = \frac{4M_1 M_2}{(M_1 + M_2)^2} E \sin^2 \frac{\theta}{2} \tag{20}$$

The nuclear stopping is calculated from the integration over all impact parameters:

$$\varepsilon_n = \frac{\langle \Delta E \rangle_n}{N \, \Delta x} = 2\pi \int_0^{b_{max}} T(\theta, E) b \, db \tag{21}$$

θ depends on the inter-atomic potential $V(r)$. When assuming target atoms as positive point charges then $V(r)$ is the Coulomb potential. However, it has to be taken into account that target atoms are screened by their electrons. After introducing a screening function ϕ with a screening length a the inter-atomic potential can be written as [14]:

$$V(r) = \frac{Z_1 Z_2 e^2}{r} \phi\left(\frac{r}{a}\right) \tag{22}$$

Here r is the distance between the nuclei, e is the unit charge and $Z_{1,2}$ are the atomic numbers of the projectile and the target atom, respectively.

The charge distribution in a solid can be approximated by Hartree-Fock calculations. However, there is no analytical expression for the inter-atomic potential function $V(r)$ that is valid for all interaction radii. Several approximations for ϕ have been derived, each valid for a certain distance between the two atoms.

When separation of the atoms is small, e.g. up to about 0.2 Å, then the screening function due to Bohr can be applied:

$$\phi\left(\frac{r}{a}\right) = e^{\frac{r}{a}} \qquad (23)$$

$$a = a_0\left(Z_1^{2/3} + Z_2^{2/3}\right)^{-1/2}$$

with the Bohr radius $a_0 = 5.29 \times 10^{-11}\ m$.

Kalbitzer and Oetzmann [15] suggested a screening function ϕ with the universal screening length a:

$$\phi\left(\frac{r}{a}\right) = \left(e + r/a\right)^{\gamma \ln\left(1+\gamma^{-1} r/a\right)} \qquad ;\gamma = \tfrac{2}{3} \quad ; e = 2.718....$$

$$a = \frac{0.8854\, a_0}{Z_1^{0.23} + Z_2^{0.23}} \qquad (24)$$

With comparable accuracy, using the same universal screening length a, Ziegler, Biersack and Littmark (*ZBL*) [16,17] found the screening function phenomenological to be:

$$\phi\left(\frac{r}{a}\right) = 0.1818\, e^{-3.2 r/a} + 0.5099\, e^{-0.9423 r/a} + 0.2802\, e^{-0.4029 r/a} + 0.02817\, e^{-0.20162 r/a} \qquad (25)$$

This universal screening potential is useful for Monte Carlo calculations. It speeds up these calculations, but discrepancies with experimental results are observed for many projectile-target combinations.

3.1.2. ELECTRONIC CROSS SECTION

The electronic energy loss of an ion penetrating a solid can have different reasons [16].

- transfer of kinetic energy from the ion to the target electrons,
- plasma oscillations or other collective behaviour of the target electrons,
- charge transfer, e.g. excitation, ionisation or electron capture of the ion.

Because of the different processes involved it is not possible to describe the stopping of ions in a solid with one single theory. Different models are applied for the different ion energies and velocities. The validity of a theoretical approach is usually given within multitudes of the Bohr velocity v_0. A hydrogen atom at 25 *keV* atom moves with a comparable velocity as its orbital electron. The corresponding energy for a helium atom is at 252 *keV*. This energy is a function of the ion's mass and atomic number. It calculates to $E = Z_1^{4/3} A_1 25\ keV$.

Slow ions ($v_1 \leq v_0 Z_1^{2/3}$) cannot transfer enough energy to electrons that are much lower than the Fermi level to excite them to an unoccupied state. In this case only electrons that are close to the Fermi level can contribute to the energy loss.

The electronic stopping reaches its maximum near $v_1 = v_0 Z_1^{2/3}$. For much higher ion velocities ($v_1 >> v_0 Z_1^{2/3}$) mainly ionisation of the target atoms takes place. The ions transfer a much higher energy to the target electrons than their binding energy ($T >> I_1$).

i. Low Ion Velocities ($v_1 \leq v_0 Z_1^{2/3}$)

For low energies ($E < Z_1^{4/3} A_1$ 25 keV) the stopping of ions in solids was calculated by Lindhard, Scharff and Schiøtt (*LSS*) [18-20]. This projectile velocity is lower than the velocity of the target electrons. *LSS* calculate the electronic stopping by assuming a free electron gas with a density ρ that changes only slightly with the location.

The electronic cross section of a particle with Z_1 is obtained by integrating all interactions I with the electron gas over all volume elements:

$$\varepsilon_e = \int I(v,\rho)\left(Z_1^*(v)\right)^2 \rho dV \qquad (26)$$

The interaction with a charged particle is treated like a perturbation of the free electron gas. Therefore effects like polarisation and screening are taken into account. The state of the projectile can deviate from Z_1 through charge transfer and is therefore replaced by the projectile's effective charge Z_1^*. Electron capture and loss are in an equilibrium which depends mainly on the velocity of the projectile.

Lindhard found that the transferred energy from the projectile to the target electron and therefore also the electronic stopping cross section is proportional to the projectile velocity:

$$\varepsilon_e = 19.2 \frac{Z_1^{7/6} Z_2}{\left(Z_1^{2/3} + Z_2^{2/3}\right)^{3/2}} \frac{v_1}{v_0} \left[\frac{eV\, cm^2}{10^{15}\, at} \right] \tag{27}$$

with the Bohr velocity $v_0 = 2.19 \times 10^6\ m/s$.

ii. Bethe – Bloch Region ($v_1 >> v_0 Z_1^{2/3}$)

The energy loss of a point charge in matter through collisions with electrons in the shell was already calculated by Bohr [21] in 1913. Bethe and Bloch [22,23] calculated quantum mechanical in Born approximation that the stopping cross section of a point charge can be obtained from:

$$\varepsilon_e = \frac{\langle \Delta E \rangle}{N\, \Delta x} = \frac{4\pi Z_1^2 Z_2 e^4}{m_e v_1^2} \left[\ln\left(\frac{2 m_e v_1^2}{\langle I \rangle} \right) - \frac{C_k(v_1)}{Z_2} \right] \tag{28}$$

where m_e is the electron mass, v_1 the velocity of the projectile, $\langle I \rangle$ the averaged ionisation potential and C_k shell corrections according to Bethe.

The main contribution for the energy loss in the Bethe – Bloch formula is from the first logarithmic term. Bloch estimated the ionisation potential $\langle I \rangle$ of the electrons to be approximately $\langle I \rangle = Z_2\ 10\ eV$ [23].

The last term $C_k\ (v_1)$ contributes shell corrections for low projectile velocities. The contribution of a certain electron shell in the target disappears when the projectile velocity is: $v_1 >> v_i$, with v_i being the electron velocity in the i-shell. This term is ~1 close to the maximum of the electronic cross section ε_e, where shell corrections come into account that limit the application of the Bethe-Bloch theory [24].

The Bethe-Bloch equation describes only the stopping of an ionised point charge correctly. Bohr [25,26] already assumed in 1940 that the projectile gets only stripped of those electrons whose classic orbital velocity is smaller than the projectile velocity. Therefore the projectile is stripped of all its electrons when $v_1 >> v_0 Z_1^{2/3}$ (Fig.4). This corresponds to a proton energy of about 250 *keV* and a helium energy of 2500 *keV*.

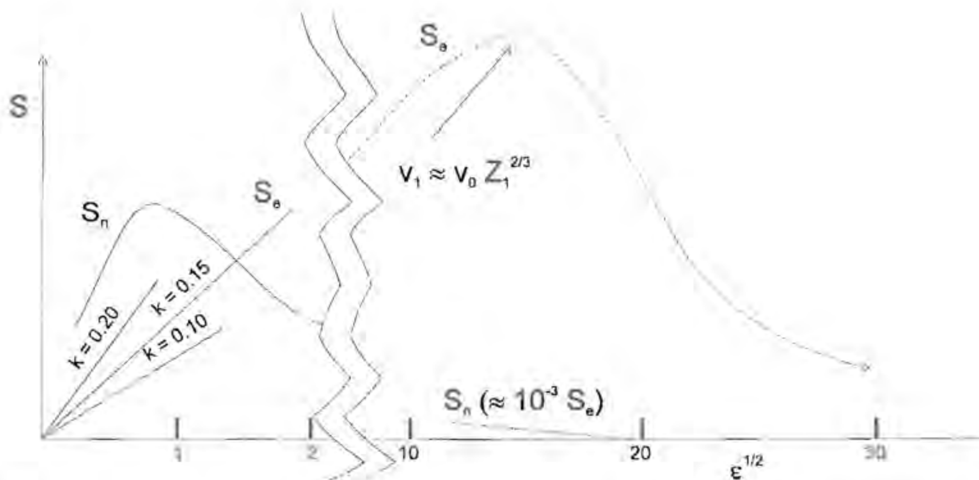

Fig.4: Nuclear (S_n) and electronic (S_e) stopping powers in reduced units versus energy in reduced units

3.2. ENERGY LOSS IN COMPOUNDS

Having a compound $A_m B_n$ of two different elements A and B one can apply a simple additivity rule on the assumption that the interaction processes between ions and component target elements are independent of the surrounding target atoms. If ε^A is stopping cross section of element A and ε^B is the stopping cross section of element B one can write for the total stopping cross section:

$$\varepsilon^{AB} = m\varepsilon^{A} + n\varepsilon^{B} \tag{29}$$

where m and n denote relative fractions of the compound materials; $m + n$ is normalised to unity. This equation is known as Bragg's rule.

The energy loss however is found to be influenced by the chemical and physical state of the medium. Deviations of the order of 10% - 20% to Bragg's rule are found in experimental results around the stopping maximum for light organic gases and for solid compounds containing heavier constituents.

A model to correct for the chemical state was developed by Ziegler and Manoyan (1988) which is called 'cores and bonds' (*CAB*) model [27]. This model assumes the energy loss of ions in compounds to be due to the cores (closed electron shell of atoms) and the chemical bonds. Some of the so calculated stopping cross sections in organic compounds can be found in ref. [27]. However, for the calculation of the *CAB* corrections one has to know the bond structure of the compound. The largest differences between the *CAB* theory and predictions for Bragg's additivity rule are found near the stopping maximum. Differences reduce with increasing energy and finally disappear at about 10 v_0.

3.3. ENERGY STRAGGLING

Charged particles loose energy through many individual encounters in a target. The number of undergone collisions and the energy transferred with each collision is due to statistical fluctuations. These fluctuations are reflected in the second moment of the stopping powers of ions in a solid. The ions have an average energy loss ΔE due to the stopping powers $S(E)$ of the target material. However, the energy distribution also widens to $\delta\Delta E$ due to:

- statistical fluctuations in the nuclear energy loss
- statistical fluctuations in the electronic energy loss
- a change of the projectile charge state causes a change of the effective charge which results in a variation of the interaction.

All the above mentioned points contribute to energy straggling.

Fig. 5 shows a sketch on how the target thickness influences the energy straggling.

UNIVERSITEIT VAN PRETORIA
UNIVERSITY OF PRETORIA
YUNIBESITHI YA PRETORIA

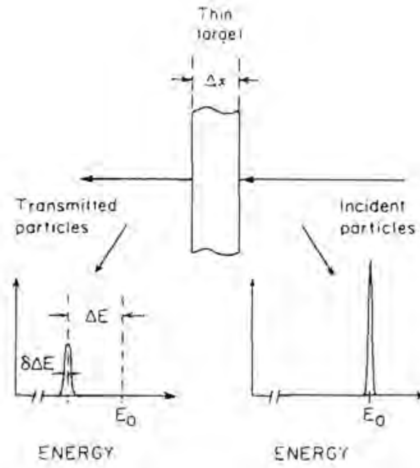

Fig.5: Influence of the target thickness on the energy loss and straggling [28].

i. Nuclear Energy Loss Straggling

The statistical fluctuations W_n^2 of the nuclear energy loss can be calculated in a similar way as the nuclear stopping by assuming a universal potential [15]:

$$W_n^2 = \int_0^\infty T^2 \, d\sigma$$
$$= 16\pi Z_1^2 Z_2^2 e^4 \frac{M_1^2}{(M_1 + M_2)^2} F_n(\varepsilon) \quad (30)$$

with: $F_n(\varepsilon) = \dfrac{1}{4 + 0.197\varepsilon^{-1.6991} + 6.584\varepsilon^{-1.0494}}$

and the reduced energy $\varepsilon = \dfrac{M_2 a}{(M_1 + M_2) Z_1 Z_2 e^2} E$

When $E \to \infty$ then the reduced energy $\varepsilon \to \infty$ and $F_n(\varepsilon) \to 0.24$. Therefore the maximum of the nuclear energy loss straggling tends to:

$$W_n^2 = 4\pi Z_1^2 Z_2^2 e^4 \frac{M_1^2}{(M_1 + M_2)^2}$$

For high projectile energies the importance of W_n^2 is negligible compared to the electronic energy loss straggling Ω_B^2.

ii. Electronic Energy Loss Straggling

Bohr [29,30] used the same assumptions as in the Bethe – Bloch equation to derive the electronic energy loss straggling. For a point charge with a high velocity he got the relation:

$$\Omega_B^2 = 4\pi Z_1^2 Z_2 e^4 N\Delta x = W_e^2 \, N \, \Delta x \tag{31}$$

Ω_B^2 is called Bohr straggling. It is the variance of the average energy loss of a projectile after passing through a layer of thickness Δx. For the number of independent collisions of the projectile with the target electrons Bohr assumed a Poisson distribution. From this a Gaussian energy loss distribution is obtained with a half width of Γ_B (with $\Gamma_B^2 = 8 \ln 2 \, \Omega_B^2$).

3.4. RANGE AND RANGE STRAGGLING

The range straggling is the second moment of the range distribution. The total range $R = \sum l_i$ is the total distance that the particle travelled in the target as schematically seen in Fig.6. The projected range is defined as the mean depth from the target surface at which the ion comes to a halt.

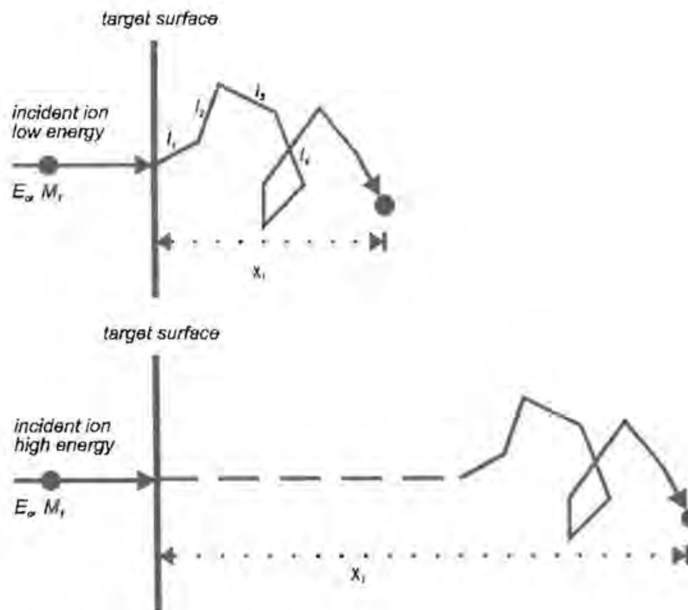

Fig.6: Range concepts for incident ions with low and high energies in a target material.

An ion incident onto a target changes its trajectory during collisions with target atoms until it comes to rest. Although the initial ion energy is fixed the number of collisions in a certain depth varies for every ion. The total distance travelled into the target is determined by the stopping powers.

The mean projected range R_p of the statistical distributed atoms after the implantation is calculated from:

$$R_p = \frac{\sum_i x_i y_i}{\sum_i x_i} \qquad (32)$$

Here y_i stands for the number of particles stopped in $\Delta x = x_i - x_{i-1}$. The second range moment ΔR_p of the distribution is calculated from:

$$\Delta R_p = \sqrt{\frac{\sum_i (x_i - R_p)^2 y_i}{\sum_i y_i}} \qquad (33)$$

This is also the standard deviation from the mean range R_p.

i14643042
b14353921

CHAPTER 4

NUCLEAR REACTION ANALYSIS (NRA)

Nuclear Reaction techniques for analysing near surface regions of solid samples are a convenient tool and have several advantages over other methods like Rutherford Backscattering (RBS) [31]. Nuclear reactions are isotope specific with no direct relationship between the mass of the target nucleus and the energy of the detected particle. Therefore light isotope tracing is possible even in heavy targets.

For NRA particles such as protons, alphas or deuterium are incident onto a target surface. When the particle penetrates the target with an energy that is high enough to overcome the Coulomb potential barrier V_C of the target nuclei it can induce a nuclear reaction. The Coulomb barrier is proportional to Z_1Z_2/R where $R = r_0\,(A_1^{1/3} + A_2^{1/3})$ with $r_0 \approx 1.25\,fm$. The nucleon numbers of the projectile and the target atoms are given by A_1 and A_2, respectively. Z_1 and Z_2 are the corresponding atomic numbers.

The barrier height for incident protons onto ^{27}Al calculates to $V_C = 3.74\,MeV$ [32]. Such high energies cannot be reached with our Van de Graaff accelerator. However, nuclear reactions can already be induced at lower energies due to tunneling effects of the projectile.

The barrier height becomes lower for decreasing atomic numbers, which makes *NRA* a suitable method to analyse light isotopes that are usually difficult to be detected by other methods.

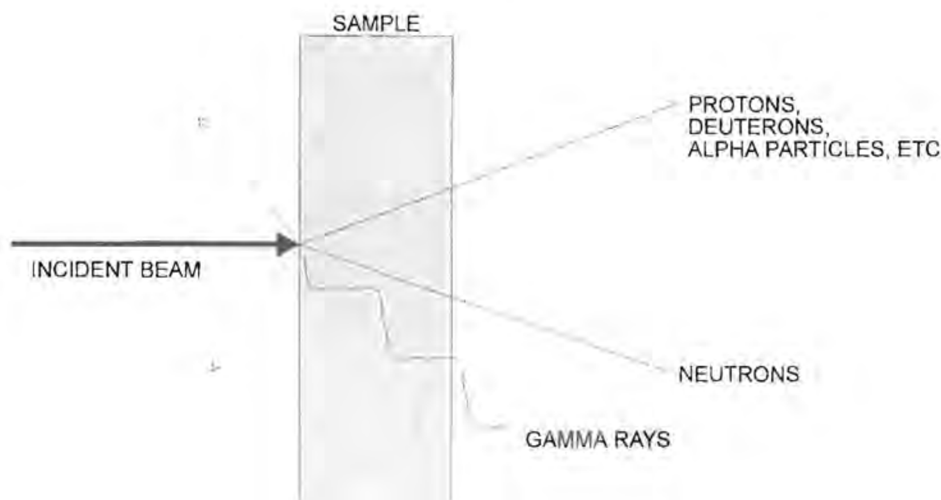

Fig.7: Schematic drawing of an incident ion beam onto a target with the various nuclear reaction products.

4.1. NUCLEAR REACTIONS

Fig.7 displays a schematic diagram of an incident beam onto a target and its resulting reaction products. When a particle a hits a target nucleus A different processes can take place:

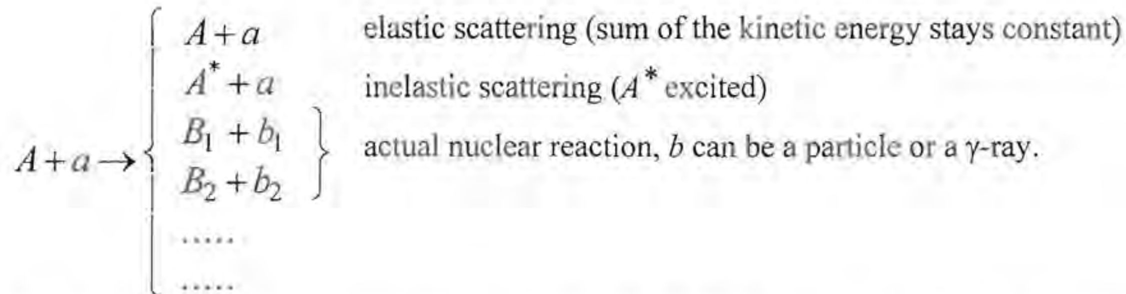

Usually a reaction is written in the form $A(a,b)B$. With the exception of the elastic scattering every resulting particle b shows an energy spectrum that contains information about the energy levels of the nucleus B. The angular distribution of the reaction particles holds information about the reaction mechanism.

Of interest for depth profiling with NRA are prompt reactions where the resulting radiation occurs instantaneously during irradiation, in contrast to activation techniques where the radiation is detected after irradiation. The resulting radiation is usually a gamma ray, a charged nuclear particle, a neutron or an electron.

4.2. ELECTROMAGNETIC TRANSITIONS

When a nucleus is in its ground state all its nucleons are in their lowest possible energy state that is allowed according to Pauli's principle. Similar to the atomic shell the state of a nucleus can be excited through energy transfer. The excitation can be the result of a single nucleon or several nucleons that are lifted from their ground state to a higher level. This can be caused by a radioactive fission, a nuclear reaction or by electromagnetic excitation from outside. When the excited state is a bound state the nucleus can only decay to its ground state by electromagnetic transition, which usually happens through the emission of a γ-ray. However, angular momentum and parity of the nucleus have to be conserved during this transition.

The eigenfunction of a nuclear state and its radiation field can be described by its angular momentum and parity eigenfunctions. Multipole fields are obtained from calculating the transition between two angular momentum eigenstates due to the conservation. These multipole fields are classified by the order l, which is an integer. For example, the lowest order l =1 is called dipole radiation.

One can distinguish between electric and magnetic multipole radiation. It is therefore customary to specify the kind of radiation field and the order l of the multipole. The terminology used is *M1* for a magnetic dipole transition and *E2* for an electric quadrupole transition.

The sum of the spins of the initial and final nuclear states $\vec{I}_1$, $\vec{I}_2$ and $\vec{l}$ of the emitted γ-ray stays constant due to conservation of the angular momentum. This leads to the following selection rules:

$$|I_1 - I_2| \leq l \leq I_1 + I_2 \quad ; \quad m = m_1 - m_2 \tag{34}$$

However, only transitions with low l are observed experimentally and in most cases the selection rules reduce to:

$$l = |I_1 - I_2| \tag{35}$$

During the emission process the parity must also be conserved which leads to additional selection rules. From the transformation characteristics of multipole fields one can deduce from the parity transformation $\vec{r} \rightarrow (-\vec{r})$ that the electric multipole radiation has the parity $(-1)^l$ and the magnetic multipole radiation has the parity $(-1)^{l+1}$. Therefore a transition can only take place when the parity π of the nuclear states before and after emission obey the following selection rules:

$$\pi_1 = (-1)^l \pi_2 \qquad \text{for } El \text{ radiation} \tag{36}$$

$$\pi_1 = (-1)^{l+1} \pi_2 \qquad \text{for } Ml \text{ radiation} \tag{37}$$

The emission of a γ-ray during an electric multipole transition causes the same parity change as an emitted particle with the angular momentum l.

change of spin $\|\Delta I\|$		0 no 0→	1	2	3	4	5
change of parity	yes	*E1* *(M2)*	*E1* *(M2)*	*M2* *E3*	*E3* *M4*	*M4* *E5*	*E5* *(M6)*
	no	*M1* *E2*	*M1* *E2*	*E2* *(M3)*	*M3* *E4*	*E4* *(M5)*	*M5* *E6*

Table 1: Multipole order of γ-transitions

The lowest multipole orders possible at a γ-transition for a given spin and parity are listed in table 1. Because of parity conservation there can never be E and M radiation of the same multipole order be emitted together. The transition probability is usually much smaller for magnetic radiation than for electric radiation of the same multipole order. With the selection rules it is possible that an *E2* and *M3* radiation can be emitted together. However, the *M3* radiation has a very small transition probability compared to the *E2* radiation. During a transition with $\Delta I = 1$ (no parity change) the transition probability of *E2* radiation is of the same order of magnitude as the *M1* radiation.

The quantum mechanical calculation of the transition amplitude is quite involved and is described in ref. [33].

In Fig.8 the calculated probabilities for different multipole transitions are sketched as a function of γ-energies for $A = 100$, $S = 1$ and $r_0 = 1.2\,fm$. At a γ-energy of 0.5 MeV the half times for transitions varies between 10^{-14} s (*E1*) and 10^{8} s (*E5*, *M5*). These calculations are only an approximation for the real interactions in a nucleus. The experimental values are usually slower by a factor 10^{3} to 10^{7} for the *E1* transition and faster by a factor of 10^{2} for the *E2* transition. The values of the other transitions are in the right order of magnitude.

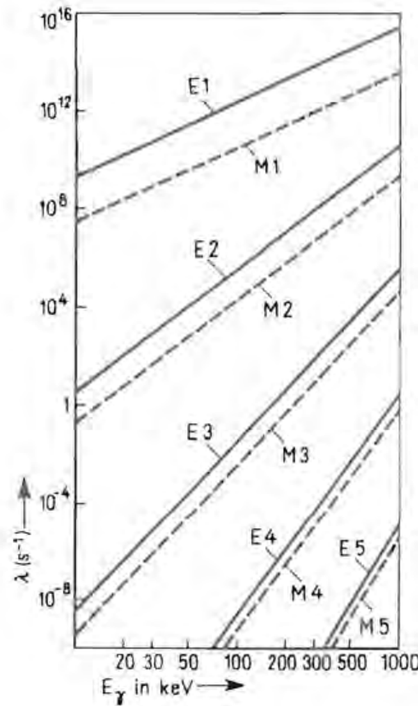

Fig.8: One particle transition probability calculated for different kinds of multipole radiation [34].

4.3. DEPTH PROFILING BY USING NARROW RESONANCES

Most of the light nuclei ($Z < 30$) have strong, sharp resonances in the cross section $\sigma(E)$ of the nuclear reactions, induced mainly with protons at low bombarding energies (< 3 MeV). Here the discussion is limited to resonances leading to prompt γ-ray emission.

When resonance reactions are used for depth profiling, the resulting γ-rays of the resonance reaction are counted versus the beam energy while the energy of the analysing beam is incremented, starting just below the resonance. The profiled depth is typically limited to a few microns.

An example for this method can be given by assuming a flat, laterally uniform sample that contains a homogeneous distribution $C(x)$ of an isotope of the element to be analysed. While bombarding the sample perpendicular to the surface with the analysing beam the induced γ-ray emission is detected. For beam energies lower than the ones required for the reaction the measured yield corresponds to background readings. After incrementing the beam energy to the one required the nuclear reactions can be induced at the surface of the sample. For higher beam energies the particles cannot induce a reaction at the surface of the sample. They get

slowed down within the target until they reach a certain depth x in the sample with the necessary energy for the nuclear reaction. As already discussed (chapter 3) the depth can be correlated to the energy loss of the projectile through the stopping powers of the target material. If the investigated isotopes are located in this depth the nuclear reaction can be induced. The detected γ-yield for this beam energy corresponds to the isotope concentration at this depth. The excitation curve of the resonance reaction $Y(E_b)$, where E_b stands for beam energy, gives an estimate of the isotope concentration distribution as a function of depth.

The depth x is correlated with the energy loss of the particles of the incident beam $(dE / dx)_{in}$ through the equation:

$$E_b = E_R + \left(\frac{dE}{dx}\right)_{in} \frac{x}{\cos\theta_1} \qquad (38)$$

where θ_1 is the angle between the surface normal and the incident particle and E_R is the projectile energy where the resonance occurs. The energy loss $(dE / dx)_{in}$ can be approximated as constant within the small energy interval $E_0 \leq E \leq E_R$ (surface approximation).

4.3.1. DEPTH RESOLUTION

The experimental resonance width is broadened due to the natural width of the resonance, the energy resolution of the beam, and the energy straggling of the beam particles during the energy loss E_b - E_R. In order to deduce the precise shape of the actual concentration profile $N(x)$, the shape of the resonance cross section $\sigma(E)$, the energy distribution of the beam $g(E_b, E)$ and the energy straggling $f(E, E', x)$ of particles at depths x have to be taken into account. The excitation curve of the resonance reaction $Y(E_b)$, i.e. the yield of the reaction vs. the bombarding energy gives an estimate of the concentration distribution [35]:

$$Y(E_b) = K\int_0^\infty dx \int_0^\infty dE \int_0^\infty dE' N(x) g(E_b, E) f(E, E', x) \sigma(E') \qquad (39)$$

K is a constant for given detection conditions. If the resonance is narrow and the beam energy resolution good, the functions g, f, and σ are sharp and therefore the yield curve corresponds well to the actual distribution.

The depth resolution depends on experimental parameters like the energy spread of the incident beam ΔE_b, the resonance width of the used reaction ΔE_R, the widening of the analysing beam energy $\Delta E_{ew}(x)$ in the depth x and the Doppler broadening ΔE_D due to the thermal motion of the reactant target atoms. By using a Gaussian approximation the total depth resolution as a function of the depth is obtained:

$$d(x) = \frac{\Delta E_{tot}(x)}{S(x)} \tag{40}$$

where:

$$\Delta E_{tot}(x) = \sqrt{\Delta E_b^2 + \Delta E_D^2 + \Delta E_R^2 + \Delta E_{ew}^2(x)} \tag{41}$$

In the set-up used for the experiments the accelerator energy beam spread was about 1 keV. In comparison to this the Doppler broadening and the resonance width of the $^{27}Al(p,\gamma)^{28}Si$ of about 105 eV are negligible.

The computer code PROFIL [36] corrects the obtained yield curves for straggling and instrumental resolution. In the first step this program calculates a depth profile from the experimental data, ignoring any energy resolution effects. It then computes from this concentration profile the expected shape of the spectrum, taking into account the determined resolution function. The difference between the calculated and experimental spectrum is then subtracted from the experimental spectrum and a new concentration profile is computed. This algorithm is repeated until the calculated spectrum coincides with the original experimental data within a given accuracy.